2019

Analytic modeling of eccentric binary black holes : from inspiral to merger

Dillon Paige Buskirk
dillonbuskirk96@gmail.com

ANALYTIC MODELING OF ECCENTRIC BINARY BLACK HOLES: FROM INSPIRAL TO MERGER

A thesis submitted to
the Graduate College of
Marshall University
In partial fulfillment of
the requirements for the degree of
Master of Science
in
Physics
by
Dillon Paige Buskirk
Approved by
Dr. Maria Hamilton, Committee Chairperson
Dr. Que Huong Nguyen
Dr. Andre Wehner

MARSHALL UNIVERSITY
DECEMBER 2019

We, the faculty supervising the work of Dillon Paige Buskirk, affirm that the thesis, ANALYTIC MODELING OF ECCENTRIC BINARY BLACK HOLES: FROM INSPIRAL TO MERGER, meets the high academic standards for original scholarship and creative work established by the Department of Physics and the College of Science. This work also conforms to the editorial standards of our discipline and the Graduate College of Marshall University. With our signatures, we approve the manuscript for publication.

Dr. Maria Hamilton, Department of Physics	Committee Chairperson	Date
Dr. Que Huong Nguyen, Department of Physics	Committee Member	Date
Dr. Andre Wehner, Department of Physics	Committee Member	Date

TABLE OF CONTENTS

LIST OF FIGURES

ABSTRACT

The orbital evolution of black hole binaries is described by two main phases: the inspiral and the merger. Using the post-Newtonian (PN) theory for the inspiral phase of the binary, we build up a Mathematica script to obtain strain waveforms for the inspiral. We expand our previous inspiral formulation to include eccentric orbits, which greatly complicates the calculations. Since this model breaks down as the two bodies approach merger, a separate model for the merger and ring-down is required. This part of the evolution is highly non-linear and numerical relativity (NR) is required to simulate this problem. However, this is computationally expensive, so an effort to create an analytic formulation that gives results comparable to NR simulations is essential in gravitational wave modeling. Our previous work used the generic implicit rotating source (gIRS) formulation, but since then another analytic model has been introduced called the Backwards-one-body (BOB) approach. This model is chosen because it builds the waveform based on the physical principles of the problem. We build a BOB model and check to see how it compares with the gIRS model. A complete waveform is built by matching the merger models with the inspiral model when it begins to break down. We compare our model with the Simulating Extreme Spacetimes (SXS) data produced using numerical relativity simulations and find great agreement.

CHAPTER 1

INTRODUCTION

The problem of developing templates for gravitational waves is of great importance since it allows us to extract information about the source of the signal. Detectable gravitational wave signals are produced through the orbital evolution of stellar massive compact binaries, such as black holes or neutron stars. The binary loses orbital energy through the emission of gravitational radiation and the orbit shrinks, increasing the frequency and amplitude of the emitted gravitational wave until the two bodies merge and the emission of gravitational radiation stops. This rapid increase in frequency near the merger is known as the "chirp" of the gravitational wave signal and is what ground-based observatories are sensitive to. It may seem like a rare scenario that two black holes or neutron stars lock each other into a collapsing orbit. These bodies are created from the remnants of stars massive enough to collapse into neutron stars (NS) or stellar-mass black holes (SBH). However, stars massive enough to result in SBH/NS ($M_{star} > 10M_{\odot}$) are found in binary systems 70% of the time [8]! The evolution and dynamical processes of black hole binary (BBH) systems is a deep subject discussed in great detail in the lecture notes of reference [8].

LIGO and VIRGO began their third observation run (O3) on April 1st, 2019 and gathers detections at a much higher frequency than previous runs, at a rate of one detection every few days. Before this observation run, it had been offline since August of 2017. This down time allowed for many improvements to the ground-based detectors, updating things like the quality of the mirrors and specifications of the lasers. The results of these upgrades gave the detectors a large increase in sensitivity, allowing for detections even further away and giving the ability to locate the source of signal with higher accuracy. The knowledge of quantum mechanics allows for the manipulation of the uncertainty

relation between the phase and amplitudes of the lasers used for detection. Timing of the laser is essential for gravitational wave detectors. The phase uncertainty of the photons is reduced or "squeezed" to allow for timing that is more precise than the standard quantum limit. These "squeezed states" of light still obey the uncertainty principle by increasing the uncertainty in the amplitude, a parameter that is not crucial for detections. The detections published up until now described circularized binaries, but this is not necessarily because they had zero eccentricity. LIGO and VIRGO had not reached sensitivity levels that allowed for the observation and confirmation of small eccentricities [12]. As our ground-based detectors become more advanced and gain the ability to be sensitive to small eccentricities, complete and accurate gravitational wave templates that are valid for small to moderate eccentricities will be essential for confirming any detections of binaries that show characteristics of eccentric orbits. This wider range of signals we expect to receive highlights our reasoning for expanding our previous model by adding corrections for eccentric binaries in their inspiral phase. In the near future, an improved detector called Cosmic Explorer will replace LIGO and will be sensitive enough to detect eccentric binaries.

CHAPTER 2

KEPLER'S PROBLEM

To understand the intensive calculations for modeling gravitational waves emitted by binary black holes (BBH) with eccentric orbits, it will be helpful to review Kepler's problem. For a binary system with masses m_1 and m_2, and total mass $M = m_1 + m_2$, it is necessary to describe the motion by reducing the two-body problem to a Keplerian one-body problem to obtain analytic solutions for Newtonian gravity. Reducing the problem following the effective one-body description allows us to only have to describe the motion of one body instead of two, in an equivalent form. For a binary in a circular orbit, a visualization of reducing the problem is shown in Figure 1.

This visualization applies to elliptical orbits where the first body is at the center-of-mass (CM) and has mass M. This body remains stationary, located at the principle focus of the ellipse as shown on the left side of Figure 2. The body in motion has the reduced mass $\mu = \frac{m_1 m_2}{M}$ and an elliptical orbit, moving in the gravitational field caused by the CM. We consider an auxiliary circle, whose origin is the center of the ellipse, with radius equal to the length of the semi-major axis of the ellipse which we denote a. The eccentric anomaly, u, is the angle from the semi-major axis to the position of the reduced mass, μ, when projected on the auxiliary circle; this is determined by drawing a perpendicular line going from the semi-major axis, through the actual position of μ on the ellipse, to the fictitious circle, and is shown on the right side of Figure 2.

In Newtonian gravity, the eccentricity is only dependent on the ellipticity of the orbit. We define the Keplerian eccentricity in equation (2.1).

$$e_K = \frac{r_+ - r_-}{r_+ + r_-} \tag{2.1}$$

The terms r_+ and r_- in equation (2.1) correspond to the distances from the CM to the

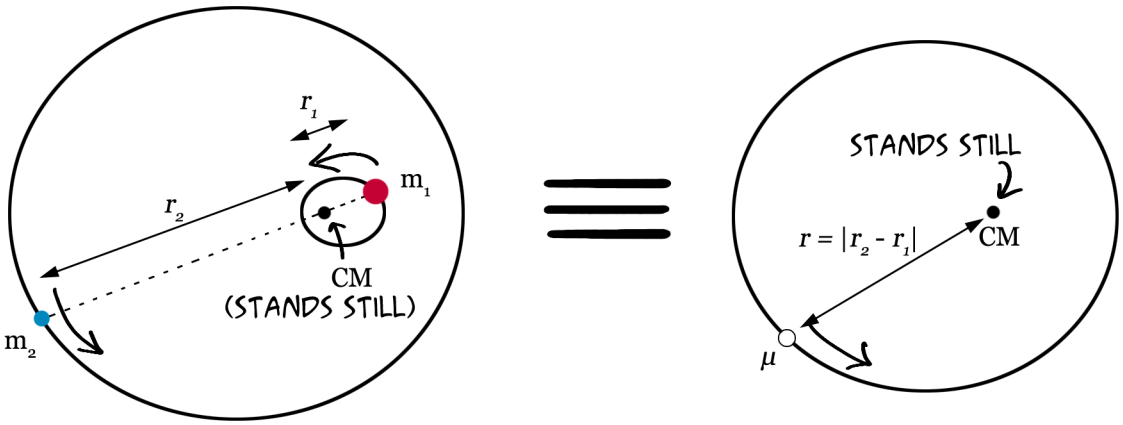

Figure 1: **Circular Effective-One-Body**.
Reducing the two-body problem to a single circular Keplerian orbit which has solutions to Einstein's equations. (Figure from
https://quantumredpill.files.wordpress.com/2013/01/two-body-cm-systems.png)

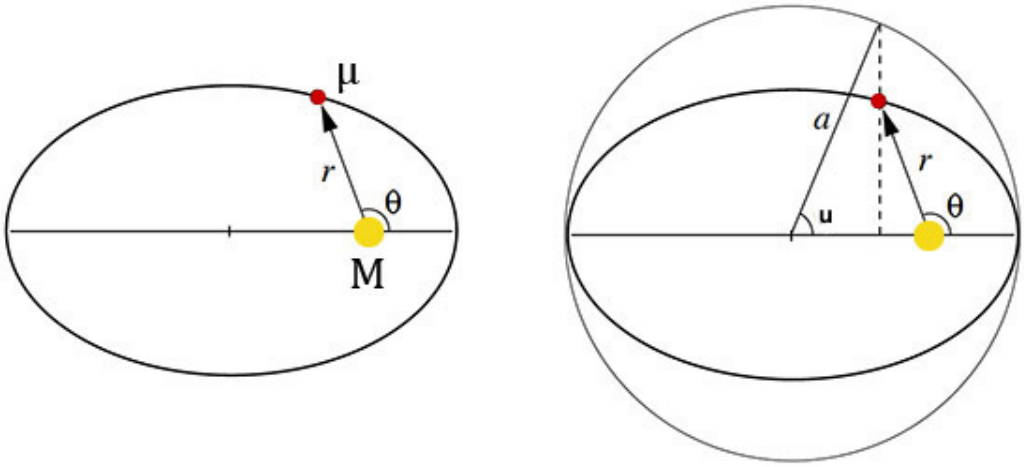

Figure 2: **Eccentric Effective-One-Body**.
The left shows the position of the masses for the eccentric, reduced mass case of Figure 1. On the right we have a visualization of the angle called the eccentric anomaly u, which evolves as the reduced mass orbits. (Figure with code from
https://matlab-monkey.com/astro/keplerEquation/KeplerEquationPub.html)

apocenter and to the pericenter of the ellipse. The apocenter is the distance from the CM to the point where the orbiting, reduced mass is furthest away from the CM. The pericenter is the point of closest approach. The Keplerian formalism, with eccentricity as the Keplerian eccentricity e_K, can completely describe the orbital motion of the binary through the separation between the fictitious bodies r_K and their relative phase ϕ_K as a function of the eccentric anomaly u [12]. The separation of the bodies within Kepler's problem has the solution given by equation (2.2), and their relative phase is given by equation (2.3).

$$r_K = a(1 - e_K \cos u) \tag{2.2}$$

$$\phi_K = 2 \tan^{-1} \left[(e_K)^{1/2} \tan \left(\frac{u}{2} \right) \right] \tag{2.3}$$

The positions of the actual bodies m_1 and m_2 in the binary can be recovered from the separation r_K in equation (2.2).

$$|r_{1,2}| = r_K \left(\frac{m_{1,2}}{M} \right) \tag{2.4}$$

Equation (2.4) gives the location of each body with respect to the center of mass M [14].

2.1 Kepler's equation

To determine how the binary evolves with time, we must know how the eccentric anomaly u can be mapped to units of time. The famous Kepler's equation (2.5) gives us a relation between the mean anomaly l and the eccentric anomaly.

$$l = u - e_K \sin u \tag{2.5}$$

The angular velocity of the orbit is variable and is called the mean motion n. The mean motion is related to the mean anomaly by $n = \dot{l}$. Since the mean motion is a function of the period of the orbit, we are able to find a relation between u and time. Finding the inversion $u(l)$ is the tricky part and involves Bessel functions of the first kind. This

problem has been on the minds of mathematicians for centuries. The eccentric anomaly (u) is one of the most challenging terms to describe in calculating the inspiral strain. This term (u) is difficult determine is due to the many Bessel functions of the first kind that appear in the summations describing the eccentric anomaly. With Mathematica we can simplify this problem with the help of the built in Bessel function command. At its core, the Bessel functions are the solution to Bessel's differential equation, a linear second-order ordinary differential equation. Differential equations that have solutions described by the Bessel function are found in many branches of physics, specifically ones that are described by wave propagation such as electricity and magnetism or Schrödinger's equation. The Bessel function of the first kind can be described by a series expansion around the origin in equation (2.6).

$$J_s(x) = \sum_{n=0}^{\infty} \frac{(-1)^n}{n!\Gamma(n+s+1)} \left(\frac{x}{2}\right)^{2n+s} \tag{2.6}$$

F. W. Bessel was a German astronomer in the early 1800s who formulated solutions to Kepler's equation as a Fourier sine series. Bessel did not have Kepler's equation in mind at first when formulating his solutions to Bessel's differential equation, but it was not long after that others realized that his work could be applied to Kepler's equation [9].

The analytic form of the eccentric anomaly that we use is given containing no relativistic corrections in equation (2.7), where $J_s(se_K)$ is the Bessel function of the first kind using the form seen in equation (2.6) [4]. We chose this form because it is accurate and easily reproducible.

$$u_{0PN} = l + \sum_{s=1}^{\infty} \frac{2}{s} J_s(se_K) \sin(sl) \tag{2.7}$$

2.2 quasi-Keplerian parametrization

However, all of this is Newtonian where the eccentricity is a parameter simply determined by the shape of the orbit. This definition of eccentricity does not hold in General Relativity because there are other factors that change the eccentricity, such as the

orbit losing energy due to the emission of gravitational waves. The two-body problem does not have analytic solutions in General Relativity so we must add perturbative corrections (known as Post Newtonian terms) to Newtonian equations of motion to obtain an analytic solution. The eccentricity becomes coordinate dependent and the approach that we chose to solve the problem of eccentric binaries in General Relativity is the quasi-Keplerian (QK) formalism. In this parameterization, the eccentricity is broken into terms: the temporal eccentricity e_t, the radial eccentricity e_r, and the angular eccentricity e_ϕ. These coordinate-based eccentricities are all related to the conserved energy and angular momentum, which means that they are not independent of each other. In calculations, it is convenient to express each coordinate-based eccentricity component in terms of a single component by using their dependence on each other. The temporal eccentricity is a common choice in many works, including our own.

CHAPTER 3

METHODS AND PROCEDURES

3.1 Eccentric Inspiral Waveforms

We implement $2PN$ and $3PN$ corrections for an eccentric binary in the inspiral phase and obtain the resultant strain. A commonly accepted quasi-circular limit for eccentricity is $e \leq 0.02$. If we find that our eccentricity approaches zero near the end of the inspiral, we can rely on our results. The only initial parameter that is required is the symmetric mass ratio, given by equation (3.1). We work with an equal mass system, such that $\eta = 0.25$ with a total mass in solar masses of $M = 1$ and eccentricity of $e_t(0) = 0.1$.

$$\eta = \frac{\mu}{M} \tag{3.1}$$

The first major step is determining the time evolution of the Post-Newtonian parameter $x \propto \frac{v^2}{c^2}$ (which adds relativistic corrections) and of the temporal eccentricity e_t [1],[10],[11]. Equations (3.2,3.3) include $3PN$ corrections and form a system of differential equations that can be solved numerically to determine x and e_t using the $NDSolve$ command in Mathematica when given initial values for both $x(0)$ and $e_t(0)$.

$$\dot{x} = \frac{1}{M}\left(\dot{x}_{0PN}x^5 + \dot{x}_{1PN}x^6 + \dot{x}_{2PN}x^7 + \dot{x}_{3PN}x^8\right) \tag{3.2}$$

$$\dot{e}_t = \frac{1}{M}\left(\dot{e}_{0PN}x^4 + \dot{e}_{1PN}x^5 + \dot{e}_{2PN}x^6 + \dot{e}_{3PN}x^7\right) \tag{3.3}$$

The PN corrections for the Post-Newtonian parameter x are given in equations (A3-A6) of reference [11], and the PN corrections for the temporal eccentricity e_t are given in equations (6.19a-6.19d) of reference [1]. The initial value for the PN parameter, x, was taken from Table 1 [10], but we have shown in our previous work that this can be calculated if we know the total mass of the binary and the low frequency limit of ground

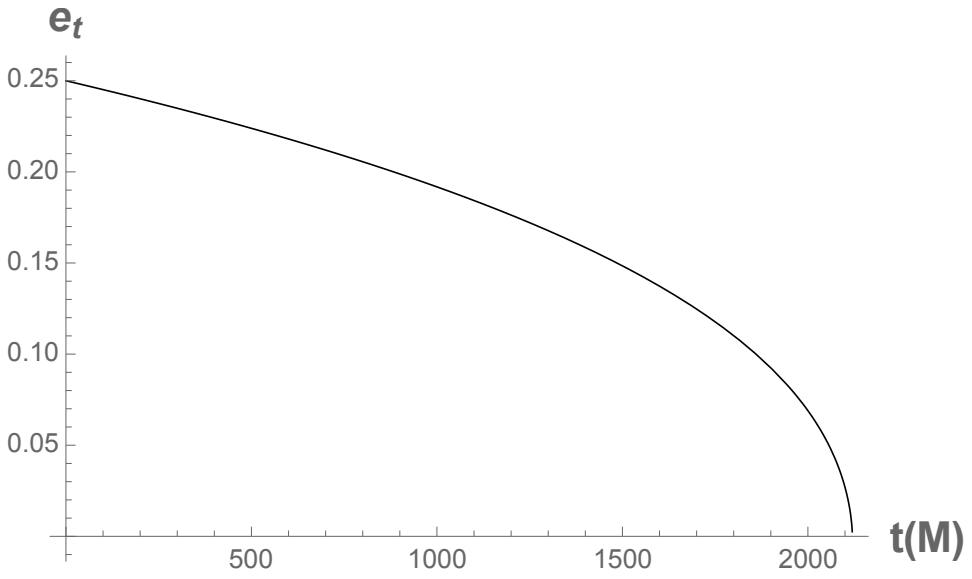

Figure 3: **Temporal Eccentricity Convergence**.
Time evolution of the temporal eccentricity e_t with initial values of $e_t(0) = 0.25$ and $x(0) = 0.0740853$. Time is given in solar masses where $1M = 4.93\mu s$. At late times, the temporal eccentricity drops off swiftly showing that the binary reaches circularization near the end of its inspiral.

based detectors [7]. The initial eccentricity can range anywhere from $e_t(0) = 0$ to $e_t(0) = 0.3$. We check that the eccentricity does approach zero at late times in the inspiral phase (near the merger) in Figure 3. This tells us that our model is ready to be matched with a merger model since a key assumption of merger models is quasi-circularization.

The resultant functions for the PN parameter x and temporal eccentricity e_t become "stiff" and the numerical method used by Mathematica is no longer applicable at a time that is close to the start of the merger when the inspiral model begins to break down. We consider this to be the final time of the inspiral, t_{fin}. Before the implementation of the $3PN$ equations, we first obtained results for the $2PN$ corrections. We discovered that we can push the equations closer to the merger when we include higher order corrections, which tells us that $t_{fin}^{2PN} < t_{fin}^{3PN}$. At early times, the $3PN$ and $2PN$ corrections give similar results. However, the closer to the merger that we push the equations, the larger the disagreement between the $3PN$ and $2PN$ corrections. This comparison will be shown in a

figure plotting the strains, later in this section. Merger models are limited in their ability to describe the strain waveform at the late inspiral, so we are required to push the inspiral calculations as far as we can to match with the merger. The limitations of merger models highlights the importance of obtaining and implementing high order corrections since they allow us to more accurately describe the terms at times near the merger.

The next step is to determine the eccentric anomaly, u. This term is complex and contains Bessel functions of the first kind and the mean anomaly l [4]. Our $3PN$ form of u is given by equation (3.4).

$$u = l + \sum_{s=1}^{\infty} A_s \sin sl \tag{3.4}$$

The Bessel functions previously mentioned for the eccentric anomaly are contained within the term A_s given by equation (3.5).

$$A_s = \frac{2}{s} J_s(se_t) + \sum_{j=1}^{\infty} \alpha_j \left[J_{s+j}(se_t) - J_{s-j}(se_t) \right] \tag{3.5}$$

It can be seen in this equation that the $0PN$ term present in equation (2.7) is contained within A_s. The coefficient α_j varies depending on the chosen coordinate system. The Arnowitt-Deser-Misner (ADM) coordinates form of α_j is given by equation (3.6), and the modified harmonic (MH) form is given by equation (3.7) up to the $2PN$ order. We omit the $3PN$ corrections in this paper due to their length. Equations (18a & 18b) in reference [4] give α_j including the $3PN$ corrections, which is what we use in our calculations.

$$\alpha_j^{ADM} = \beta_t^j \left[x^2 \left(\frac{15 - 6\eta}{j\sqrt{1 - e_t^2}} - \frac{4\eta + \eta^2}{4} \right) \right] \tag{3.6}$$

$$\alpha_j^{MH} = \beta_t^j \left[x^2 \left(\frac{15 - 6\eta}{j\sqrt{1 - e_t^2}} - \frac{15\eta - \eta^2}{4} \right) \right] \tag{3.7}$$

The term β_t is a function of the temporal eccentricity given by equation (3.8) and is useful

in writing α_j in a simpler form.

$$\beta_t = \frac{1 - \sqrt{1 - e_t^2}}{e_t} \tag{3.8}$$

Comparing the strain of each coordinate system, there is no visual difference. However, closer to the merger a small difference between the two arises, but this difference is negligible.

The last term we need to describe the eccentric anomaly, u, is the mean anomaly, l, which is related to u through Kepler's equation. As discussed in Section (2.1), the mean motion is related to the mean anomaly by $n = \dot{l}$ and is given by equation (3.9) up to the $3PN$ order.

$$n = \dot{l} = \frac{1}{M}\left(x^{3/2} + n_{1PN}x^{5/2} + n_{2PN}x^{7/2} + n_{3PN}x^{9/2}\right) \tag{3.9}$$

The PN corrections for the mean motion n are given in equations (A2-A4) in reference [10]. Integrating this result gives the mean anomaly, providing us with all of the pieces needed to describe the eccentric anomaly analytically.

The computational cost of evaluating the eccentric anomaly u is so large that it requires several minutes to evaluate. This long computation time is not ideal because u appears many times in other terms leading up to the strain waveform, causing the script to not run in a reasonable amount of time. The upper bound of relative error caused by computer precision is known as machine epsilon ($\epsilon_m = 2.22 \cdot 10^{-16}$). We want to decrease the time of evaluation to have it running in seconds instead of minutes without sacrificing the accuracy of the script by having a relative error in the realm of ϵ_m. The first step to decreasing the evaluation time is to determine the upper limit of the summations in equations (3.4 & 3.5), since the Bessel functions contained within the sums are computationally expensive. After comparing the accuracy and computation time of different truncation values, we decided to choose $j, s = 1, 2, ..., 8$ for our truncation value. Truncating the sums at this value allows u to be evaluated with the desired accuracy, but still not near the desired time of a couple seconds. We developed a method that allows us

to only have to evaluate u once in its complex, Bessel function form. When u appears in other terms, we use a nearly equivalent polynomial form that evaluates swiftly, allowing for the script to run in a desirable amount of time. This equivalent function is obtained using a command built into Mathematica that preforms a polynomial interpolation (fitting a polynomial to a given set of data in a way that minimizes error). First, we must tabulate the values of u at every time up until t_{fin} in increments of $\Delta t = 0.2$ and create a table of the form $(t, u[t])$. This table gives us the data in a format that can be interpolated with a simple command. The four lines of code that create an interpolated, polynomial function for u out of the Bessel function form are given in Figure (13). We choose a polynomial order of 4 because this has a relative error (between the interpolated function and the Bessel function form of the eccentric anomaly) near the order of 10^{-16}. The extremely small error means that using an interpolating polynomial to describe u in future terms leading up to the strain is much faster with virtually no loss of accuracy, a highly desired feature of any problem in numerical analysis!

Before we can obtain the inspiral strain waveform, we need to determine how the separation, r in equation (3.10), and the relative angular velocity, $\dot{\phi}$ in equation (3.11), evolve in time with corrections up to the $3PN$ order.

$$r = M\left(r_{0PN}x^{-1} + r_{1PN} + r_{2PN}x + r_{3PN}x^2\right) \tag{3.10}$$

$$\dot{\phi} = \frac{1}{M}\left(\dot{\phi}_{0PN}x^{3/2} + \dot{\phi}_{1PN}x^{5/2} + \dot{\phi}_{2PN}x^{7/2} + \dot{\phi}_{3PN}x^{9/2}\right) \tag{3.11}$$

The PN corrections for the separation and the relative angular velocity are given by Hinder in equations (A6-A9) and (A11-A13) respectively [10]. The eccentric anomaly, u, appears even in the zeroth order corrections for the separation in equation (3.12), and relative angular velocity, in equation (3.13).

$$r_{0PN} = 1 - e_t \cos u \tag{3.12}$$

$$\dot{\phi}_{0PN} = \frac{\sqrt{1-e_t^2}}{(e_t \cos u - 1)^2} \tag{3.13}$$

We also require the differentiation of the separation $\dot{r}$ and integration of $\dot{\phi}$ to obtain the phase ϕ. Doing the differentiation and integration gives us the last of the terms in the strain that are not parameters left for us to choose. Integration of the angular velocity goes smoothly in Mathematica by formatting it as a differential equation that solves for the phase, ϕ. However, to obtain time derivative of the separation evolution, we must use the same trick that was used to simplify the eccentric anomaly given in the lines of code in Figure (13). Following the previously outlined method simplifies the complex form of the separation, given by equation (3.10), into a fourth order polynomial that can easily be differentiated in Mathematica. The relative error between the interpolated form of the separation and its original form is of the order the 10^{-15} which is well within our desired accuracy, which means we are able to differentiate the interpolated polynomial instead of the complex expression for r and still have reliable results.

We use the form of the strain that we calculated in our previous work [7], which assumes that the binary is optimally oriented for the detector for simplicity.

$$h = (A_1 + iA_2)e^{-i2\phi} \tag{3.14}$$

$$A_1 = -2\frac{M\eta}{R}\left(\dot{r}^2 + r\dot{\phi}^2 + \frac{M}{r}\right) \tag{3.15}$$

$$A_2 = -2\frac{M\eta}{R}\left(2r\dot{r}\dot{\phi}\right) \tag{3.16}$$

The term R is the distance from the detector to the binary system, which we can choose to be unity since we will normalize the strain amplitude. The plus and cross polarizations of the waveform are found by taking the real and imaginary parts of equation (3.14). In Figure 4 we can see the disagreement between the resultant strains, using $2PN$ corrections and $3PN$ corrections, as we approach the late inspiral into the merger. It is known that the inspiral model no longer holds true when we reach the merger. Using higher order

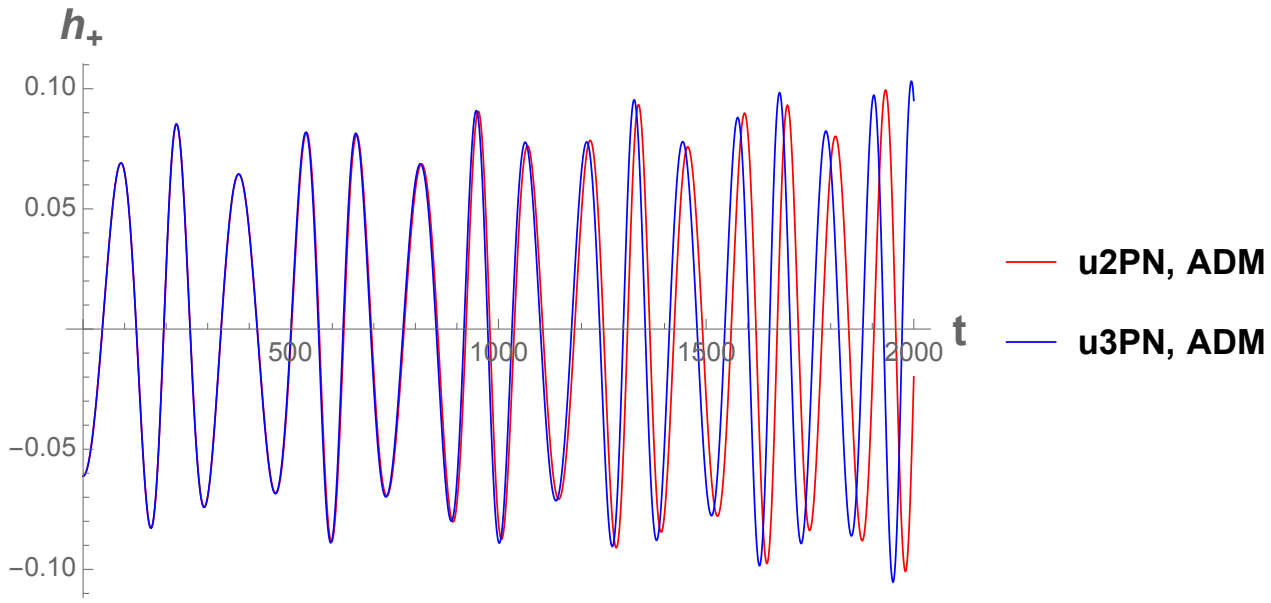

Figure 4: **2PN vs. 3PN Order Strain**.
Comparison of the unnormalized strain in ADM coordinates using $2PN$ corrections and $3PN$ corrections. The strain is cut-off at a time before t_{fin}^{3PN} since we are unable to obtain results for $2PN$ corrections at times later than t_{fin}^{2PN}. This plot is produced for the equal mass case with initial temporal eccentricity $e_t(0) = 0.1$.

corrections to the inspiral model is desired because it allows us to push the validity of the inspiral closer to a time where we can match with a merger waveform model. Merger models assume that the binary has circularized prior to merger. We can check that our inspiral model is valid, and we see that the eccentricity, $e_t(t_{fin}) \approx 0$, is close enough to zero to assume that the binary has circularized prior to matching with a merger model. We plot the real part of the strain for the eccentric binary black hole, using our parameters mentioned in the beginning of the section with time in units of solar masses in Figure 5. The strain is plotted for a variety of initial temporal eccentricities in Figure 6. The eccentricity introduces a second harmonic within the strain waveform, if compared to a circular binaries waveform like the one we look at in the next section for the first gravitational wave detection (GW150914).

In the world of GW detections, the event will rarely be optimally orientated, and thus the inclination angle θ causes the strain to vary. This is the angle between the

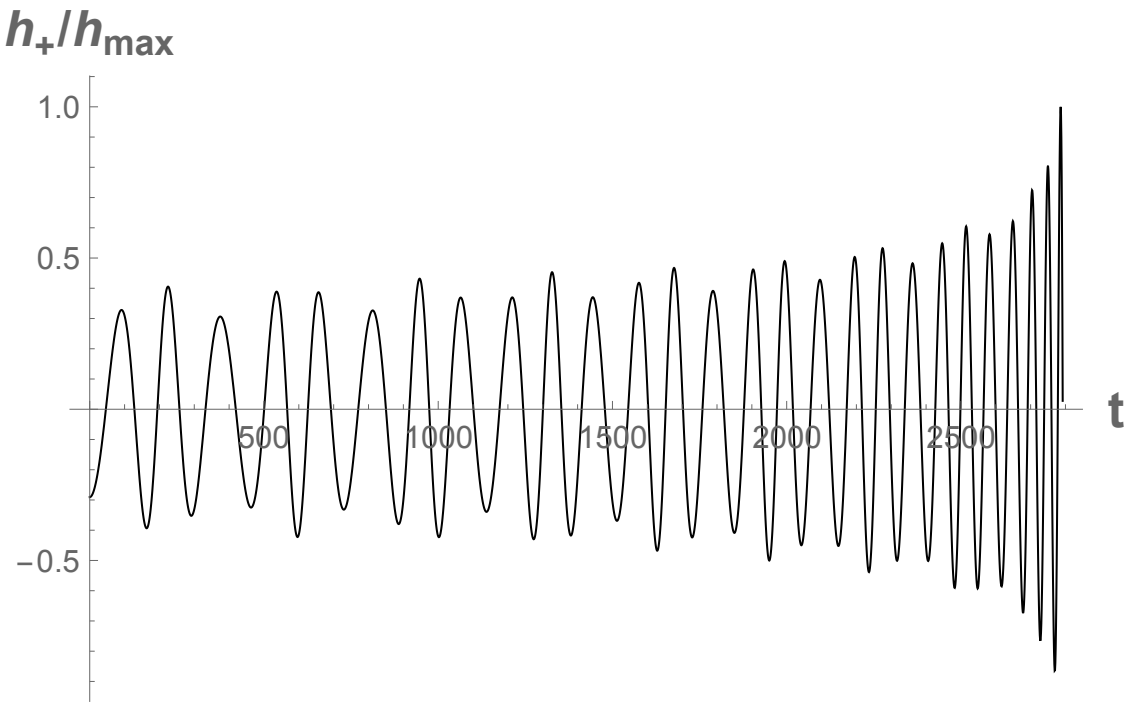

Figure 5: **Eccentric Inspiral Strain**.
The plus polarization (the real part) of the normalized strain waveform for an equal mass binary of initial eccentricity $e = 0.1$.

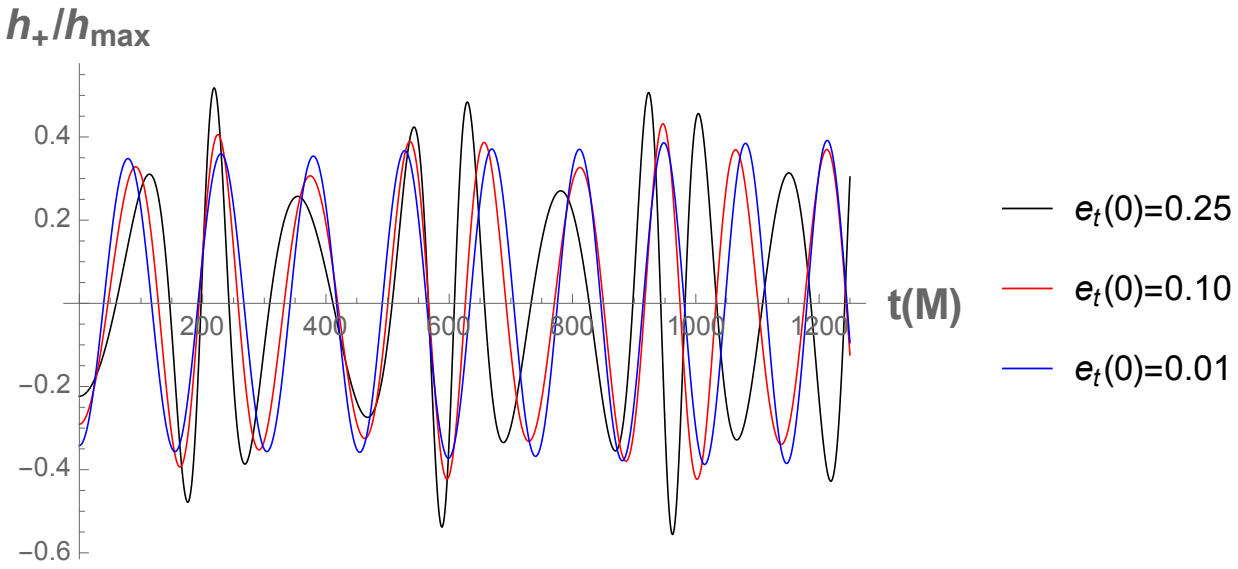

Figure 6: **Small to Moderate Eccentric Strain**.
Comparing the inspiral strain waveforms for different initial temporal eccentricity values. The higher eccentricity case introduces extra harmonic behavior later in the inspiral phase, when compared to the low eccentricity strain.

detectors plane of reference and the orbital plane of the binary. The plus and cross polarizations for the strain waveform with an adjustable inclination angle is given by equations (3.17 & 3.18) [11].

$$h_+ = -\frac{M\eta}{R}\left[\left(\cos^2\theta+1\right)\left[\cos 2\phi\left(-\dot{r}^2+r^2\dot{\phi}^2+\frac{M}{r}\right)+2r\dot{r}\dot{\phi}\sin 2\phi\right]+\left(-\dot{r}^2+r^2\dot{\phi}^2+\frac{M}{r}\right)\sin^2\theta\right] \tag{3.17}$$

$$h_x = -\frac{2M\eta}{R}\cos\theta\left[\left(-\dot{r}^2+r^2\dot{\phi}^2+\frac{M}{r}\right)\sin 2\phi\ -2r\dot{r}\dot{\phi}\cos 2\phi\right] \tag{3.18}$$

We will leave the study of the inclination angle to other work.

3.2 GW150914 Inspiral Waveform Comparisons

A good way to test the accuracy of our eccentric inspiral model is to look at it in the zero eccentricity limit and compare the results to the data available at the LIGO Open Science Center (LOSC) for the first gravitational wave detection, GW150914. The initial masses of each black hole in solar masses are $m_1 = 36.2$ and $m_2 = 29.1$. The initial value of the PN-parameter x is taken to be $x(0) = 0.04672277$, which is calculated and proven in our previous work [7]. The binary in this detection has circularized prior to being detectable, so the eccentricity is zero. Before we can compare our results to the LOSC data, we need to be certain that the zero eccentricity limit of our new inspiral model agrees with our previous publication [7]. The old model contains corrections up to the $6PN$ order when determining the post-newtonian parameter x for the quasi-circular limit, while the new eccentric model only has corrections up to the $3PN$ order and skips half-order corrections. To get these two models to agree, we must include only the corrections that our eccentric model has by taking out the half-order corrections and the corrections higher than $3PN$ from our previous circular model. Having $e_t(0) = 0$ greatly simplifies our eccentricity model and makes the eccentric anomaly, $u = 0$, for all times, which speeds up the evaluation time. Now that our models are in agreement, we need to take the necessary steps in order to have our model strains be comparable to the LOSC data. First, we choose

what cycles of the waveform that we want to compare from the LOSC data. Since the true test of the strength of an inspiral model is how accurate it is approaching the merger, we choose a peak just before merger for the LOSC data and compare results for five cycles before that peak. Similarly, for our inspiral model, we choose a peak just before the model breaks down and take data for five cycles before that peak. Up until now, we have always worked with time in units of solar masses, but the LOSC data is given in real units of time (seconds). By simply expressing the initial total mass in units of seconds instead of solar masses we see that the eccentric model and circular model produce results with time in units of seconds. This unit conversion is explained, and a conversion factor is proven in Appendix A of our previous work [7]. The last step before obtaining comparable results is to fit the amplitudes. This fit is accomplished by using a scaling factor to compare the starting peak in our data with the LOSC data. The comparison of the results from our inspiral models to the LOSC data is shown in Figure 7. We see that both the amplitude and the frequency of the strain waveform evolve the same for our previous model, the zero eccentricity limit of the model outlined in this paper, and the LOSC data for the first gravitational wave detection. This agreement shows that our results are reliable and that the zero eccentricity limit of the model in this paper gives similar results to our old model that was limited to the case of a circular binary, which convinces us that we have successfully expanded our previous inspiral model to allow for less limitations.

3.3 BOB Merger Model

The Backwards One Body (BOB) method developed in reference [13] presents an analytic approach to calculating the gravitational wave strain of a binary black hole system during the late inspiral, merger, and ringdown phases. Our reasoning for using this model is that it is the first merger model to be created analytically without the help of fitting to numerical relativity data. It is stated that this model is accurate during the "late inspiral," which refers to the time once the binary reaches the innermost stable circular orbit (ISCO) (when $r_{ISCO} = 6M$) to before it reaches the light ring at $r_{lr} = 4M$. The reason for using

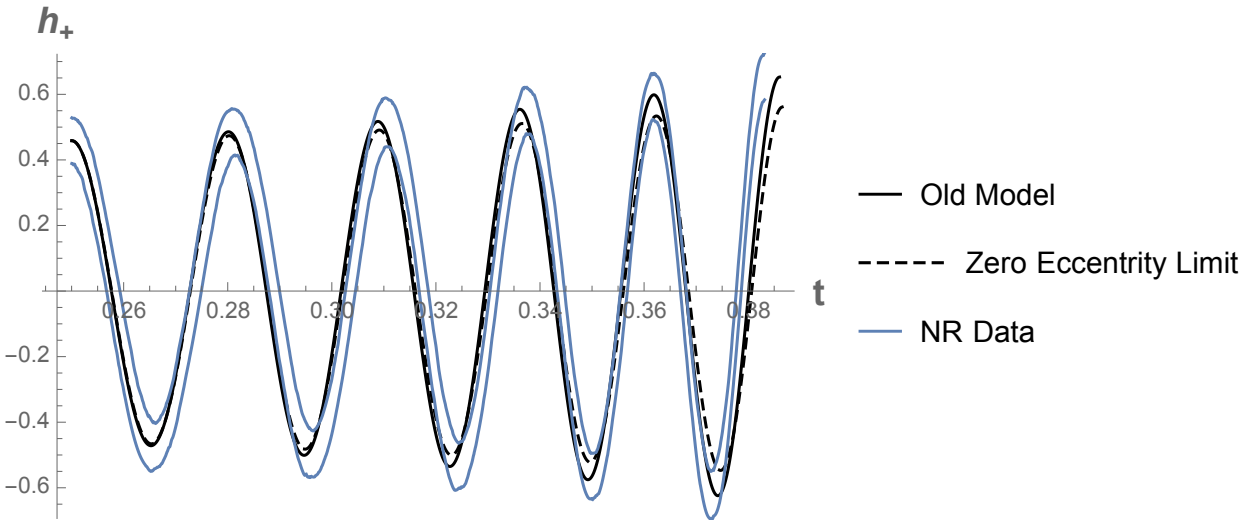

Figure 7: **GW150914 Strain**.
Comparing the numerical relativity data, available through the LOSC, of the gravitational wave detection GW150914 to the results produced from our models from plugging in the estimated initial parameters extracted from the actual signal. This is the only plot where time is expressed in units of seconds. The old model is only valid for the circular case while the eccentric model is being checked to see how it holds at the zero eccentricity limit.

the term "backwards" in BOB is due to the way the problem is modeled for calculations. This approach tackles the merger dynamics of a BBH by envisioning a single black hole, with mass and spin equal to the mass and spin of the final remnant black hole, M_{fin} and s_{fin}. The gravitational wave emissions in this picture are caused by a second, much less massive perturber that orbits the remnant black hole starting at the ISCO until it passes through the light ring. Since the final form of the remnant is known, we work backwards to determine the path that the perturber must take to describe the disturbances in spacetime leading to the stable remnant. Considering the gravitational radiation from the geometric optics perspective, it was found that the majority of the signal does not come from the perturber itself [6]. Instead, we are observing the reflections off the light ring as the perturber spirals towards the light ring from ISCO. Once the perturber passes through the light ring, the majority of the gravitational radiation caused by the perturber is absorbed into the remnant black hole. In this model, the ringdown corresponds to the higher frequency disturbances caused by the perturber passing through the light ring. Since this

passage occurs at the light ring, the high frequency perturbations emitted during the passage have greater azimuthal momentum and travel around the light ring longer, causing us to observe them at later times. The frequencies of these later signals range from the frequency of the perturber itself, to the frequency of a massless particle traveling at the light ring (the null circular orbital frequency), which corresponds to the quasi-normal mode (QNM) frequency. This condition sets an upper limit on the frequency of gravitational radiation that we can observe since perturbations with a greater frequency are trapped in the light ring and do not have enough momentum in the radial direction to escape and reach our detectors.

Our goal with this model is to build it from the ground up following reference [13] and to confirm any equations that may be unclear. Once we have built the model, we will check the accuracy of the model by comparing the results to the Simulation Extreme Spacetime (SXS) data for a nearly equal mass binary [5]. We will also compare the results with those obtained through a generic implicit rotation source (gIRS) formulation, which was the merger model we used in the past [11]. The calculations and methods for this model are found in our previous work [7].

The three key terms that we need to produce a strain are the amplitude term given by the Weyl scalar $|\psi_4|$, the orbital frequency Ω, and the phase Φ (obtained by integrating the frequency). The terms used in strain calculations are lower case and are related to the capitalized terms by $\phi_{lm} = m\Phi$ and $\omega_{lm} = m\Omega$. The capitalization of the terms is used as a way to distinguish between the rotation of the source and the terms directly related to the gravitational waves. We limit our approach to only the $l = m = 2$ mode from now on, so subscripts will be dropped.

The first term we will look at is the widely used Weyl Scalar, ψ_4. It is proportional to the second time derivative of the strain and is a key term in determining the waveform amplitude in numerical relativity codes. We work towards deriving the Weyl Scalar by starting with the evolution of the radial coordinate r in equation (3.19), which describes

the position of the perturber and is related to the path that the leading gravitational wave takes. The other coordinates are considered to be constant in time.

$$r = r_{lr}[1 + \epsilon f(t - t_p)] \tag{3.19}$$

The time t_p is when the waveform amplitude is maximum and can be freely chosen to be $t_p = 0$. The term $f(t - t_p)$ is the function of the perturbation given by equation (3.20), and ϵ is some small scaling factor that the perturbation is multiplied by.

$$f = \sinh\left(\frac{t - t_p}{\tau}\right) \tag{3.20}$$

The term τ is the dampening time of the amplitude given by equation (3.21).

$$\tau = \frac{Q}{\Omega_{QNM}} \tag{3.21}$$

The fit for the quality factor Q is given in reference [3] for different modes. For our $2, 2$ mode, Q is given as a function of the final spin, s_{fin}, shown in equation (3.22).

$$Q = 0.7 + 1.4187(1 - s_{fin})^{-0.499} \tag{3.22}$$

The quasi-normal mode frequency is also given in reference [3] for the $2, 2$ mode in equation (3.23).

$$\omega_{QNM} = \frac{1.5251 - 1.1568(1 - s_{fin})^{0.1292}}{M_{fin}} \tag{3.23}$$

In this equation, M_{fin} is the final remnant mass of the binary, and this is related to the term in the dampening time by $\Omega_{QNM} = \omega_{QNM}/2$. The values of M_{fin} and the final spin, s_{fin}, are taken from the SXS data. In the case that these values are not known, one may have to resort to numerical relativity. Since it is desirable to build a model that does not rely on NR, papers have been published containing methods for calculating the final mass

and final spin of a remnant black hole analytically [13, 2].

From geometric optics, the amplitude is shown to satisfy a transport equation given by equation (3.24).

$$\frac{d}{dt}(drA) = 0 \tag{3.24}$$

If we plug the perturbative function (3.20) into the equation for our radial component (3.19) and differentiate, we clearly see that $dr \propto \cosh\left(\frac{t-t_p}{\tau}\right)$. Performing a time integration on equation (3.24), we set it equal to some integration constant that we call A_p. Solving for the amplitude A, we obtain equation (3.25).

$$A = A_p sech\left(\frac{t-t_p}{\tau}\right) \tag{3.25}$$

The term A_p is a scaling factor that can be chosen freely to fit with the amplitude of whatever we are comparing our model to. Since we will normalize the amplitude of the final strain later on, we just set $A_p = 1$ for simplicity. The amplitude A can describe any derivative of a waveform. The source of gravitational waves is the curvature of the space-time, which is related to the second derivative of the space. General relativity describes gravitational waves in terms of the Weyl scalar $|\psi_4|$, a quantity commonly seen in numerical relativity codes. The Weyl scalar is related to the strain by $|\psi_4| = \ddot{h} \approx h\omega^2$, so we can set the amplitude of the Weyl scalar to be in the same form as the amplitude that we derived from the transport equation.

$$|\psi_4| = A_p sech\left(\frac{t-t_p}{\tau}\right) \tag{3.26}$$

Now that the form of the Weyl scalar is chosen and our amplitude is obtained, we can shift our focus to the orbital frequency of the binary. We will deduce the orbital

frequency to be in the form given by reference [13], shown in equation (3.27).

$$\Omega(t) = \left(\Omega_0^4 + k\left[\tanh\left(\frac{t-t_p}{\tau}\right) - \tanh\left(\frac{t_0-t_p}{\tau}\right)\right]\right)^{1/4} \tag{3.27}$$

In this equation, k is some constant that must be determined. We start by looking at the Bondi news, N, which is the time derivative of the strain. This quantity is related to the orbital frequency by equation (3.28) given in reference [2].

$$|N|^2 = 16\pi\xi\Omega\dot{\Omega} \tag{3.28}$$

The term $\xi = m^2\frac{dJ}{d\Omega}$ is the change in dynamical moment of inertia, which is found to be constant during the merger. Since the Bondi news is the first derivative of the strain, and the Weyl scalar is related to the second derivative of the strain, we can compare the Bondi news to the Weyl scalar to obtain the useful relationship given in equation (3.29).

$$|\psi_4|^2 = m^2\Omega^2|N|^2 \tag{3.29}$$

In this relation, we plug in equation (3.28) and (3.26) to obtain a first order differential equation for the orbital frequency that can be solved using the separation of variables.

$$\operatorname{sech}^2\left(\frac{t-t_p}{\tau}\right)dt = 16\pi m^2\xi\Omega^3 d\Omega \tag{3.30}$$

At this point, we introduce the constant k that appears in equation (3.27) by enforcing the relation shown in equation (3.31).

$$\frac{k}{4\tau} = \frac{1}{16\pi\xi m^2} \tag{3.31}$$

Doing this brings equation (3.30) to the form of equation (3.32).

$$\frac{k}{4\tau}\operatorname{sech}^2\left(\frac{t-t_p}{\tau}\right)dt = \Omega^3 d\Omega \tag{3.32}$$

The resultant differential in equation (3.32) can be trivially integrated to confirm equation (3.27). However, to determine the constant k, the limits of integrations must be carefully chosen. For the integration over $d\Omega$, we know the lower limit must be the frequency that we choose from the end of the inspiral model to match with BOB at time t_0, such that $\Omega(t_0) = \Omega_0$. The upper limit of this integration is the quasi-normal mode frequency, Ω_{QNM}, which is the frequency of the final waveforms that we detect from the ringdown of the merged binary. As the frequency evolves, it asymptotes towards the quasi-normal mode frequency so that we can consider that the frequency is equal to Ω_{QNM} at late times ($t \to \infty$). With this knowledge, the limits of integration for time are clearly seen to be from t_0 (the time that we match the inspiral model with BOB) to some final time that is far enough past the peak of the merger that it can be considered infinity. Performing the integration of equation (3.32) with the discussed limits and solving for k, we find that the constant k becomes equation (3.33) which is in agreement with equation (8) from reference [13].

$$k = \left(\frac{\Omega_{QNM}^4 - \Omega_0^4}{1 - \tanh[(t_0 - t_p)/\tau]} \right) \tag{3.33}$$

The statement that $\Omega(t)$ approaches Ω_{QNM} at late times can be checked by plugging k into equation (3.27) for a time $\Omega(t \to \infty)$. Since we choose t_p to be zero, we must determine the starting time of the merger model t_0. The matching time is found by enforcing the continuity condition that is obtained by rearranging equation (3.32). This condition was chosen so that the inspiral and merger models are in phase with each other at the matching time. At time t_0, Ω and $\dot{\Omega}$ become Ω_0 and $\dot{\Omega}_0$ respectively. These values are obtained using the frequency values from the PN inspiral model at late times, just before the model is no longer applicable. Plugging in the form of k that we determined in equation (3.33), we obtain the relation given in equation (3.34).

$$\operatorname{sech}\left(\frac{t_0 - t_p}{\tau} \right) = 2\sqrt{\frac{\tau \Omega_0^3 \dot{\Omega}_0 (1 - \tanh(\frac{t_0 - t_p}{\tau}))}{\Omega_{QNM}^4 - \Omega_0^4}} \tag{3.34}$$

Solving for t_0 from equation (3.34) is best done using Mathematica due to the t_0 terms being contained within hyperbolic functions. Mathematica, by default, considers any variable, such as t_0, to be complex. However, the solution could change depending on the domain of values that t_0 can take on, so we must limit t_0 to the real domain in Mathematica since we know time must take on real values. We then preform a solve command on equation (3.34) to obtain the result in equation (3.35).

$$t_0 = t_p + \tau \log \left[\sqrt{2} \sqrt{-\frac{\tau \Omega_0^3 \dot{\Omega}_0}{\Omega_0^4 + 2\tau \Omega_0^3 \dot{\Omega}_0 - \Omega_{QNM}^4}} \right] \tag{3.35}$$

The above equation does not coincide with t_0 given in reference [13]. However, after some logarithmic identities and simplification, t_0 can be rearranged into the elegant form seen in equation (3.36), which matches form of the equation for t_0 given in reference [13].

$$t_0 = t_p - \frac{\tau}{2} \ln \left(\frac{\Omega_{QNM}^4 - \Omega_0^4}{2\tau \Omega_0^3 \dot{\Omega}_0} - 1 \right). \tag{3.36}$$

Finally, the last key term in obtaining a strain waveform is the phase Φ. As previously mentioned, the phase is calculated through the integration of the frequency given in equation (3.27), when working in the quasi-circular limit. The result of the integration is given in a compact form shown in equation (3.37).

$$\Phi = \int_0^t \Omega dt' = \arctan_+ + \operatorname{arctanh}_+ - \arctan_- - \operatorname{arctanh}_- \tag{3.37}$$

The abbreviated trigonometric terms are given in equation (10) of reference [13] and were checked by using the integration command in Mathematica.

With the three key terms clearly derived, we can build an equation for the strain. Equation (3.38) shows how the Weyl scalar, frequency, and phase describe the evolution of the strain. The real and imaginary parts correspond to the plus and cross polarizations of the strain respectively.

$$h = \frac{|\psi_4|}{\omega^2} e^{i\phi} \tag{3.38}$$

CHAPTER 4

RESULTS

4.1 Matching

With the BOB approach programmed from the ground up using Mathematica, we can combine it with the inspiral model to produce a full waveform. The resultant merger waveform that we produced for matching considers an equal mass case where the total mass of the binary system is normalized. The final spin is chosen to be $s_{fin} = 0.686461$, and the final mass of the remnant is given as a fraction of the total mass to be $M_{fin} = 0.95174$. The real and imaginary strain waveforms using Equation (3.38) from following the BOB formulation for these parameters is shown in Figure 8. We observe the expected phase difference between the two polarizations.

In order to produce a complete waveform, we want to match the merger waveform with the end of our inspiral model. We use the zero eccentricity limit of our inspiral formulation by changing the initial eccentricity to zero the script we used to generate Figure 5, to produce the inspiral strain for matching. The inspiral model is pushed until a time just before the model breaks down. To determine where the strains will be matched, we work in the frequency domain. The plot of the matched frequencies for the late inspiral and merger is shown in Figure 9.

We then shift the inspiral waveform back in time so that the strains align as they approach the peak amplitude seen just before $t = 0$ in the real part of Figure 8. Matching in the frequency domain allows us to determine the time shift for the strain and solidifies our strain matching results. The resultant inspiral-merger-ringdown (IMR) waveform is shown in Figure 10.

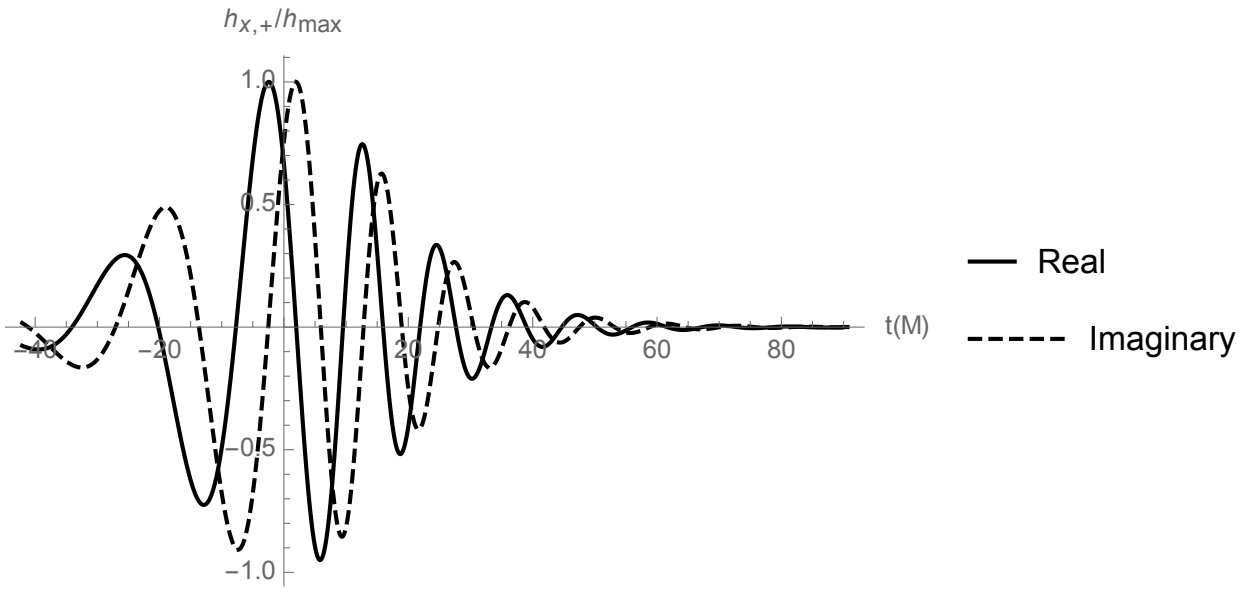

Figure 8: **BOB Merger Strain**.
The real and imaginary strain waveforms for the equal mass binary produced following the BOB formulation. The amplitude of the strain is normalized. The data is time-shifted so that the amplitude term $\left(\frac{|\psi_4|}{\omega^2}\right)$ peaks at time zero.

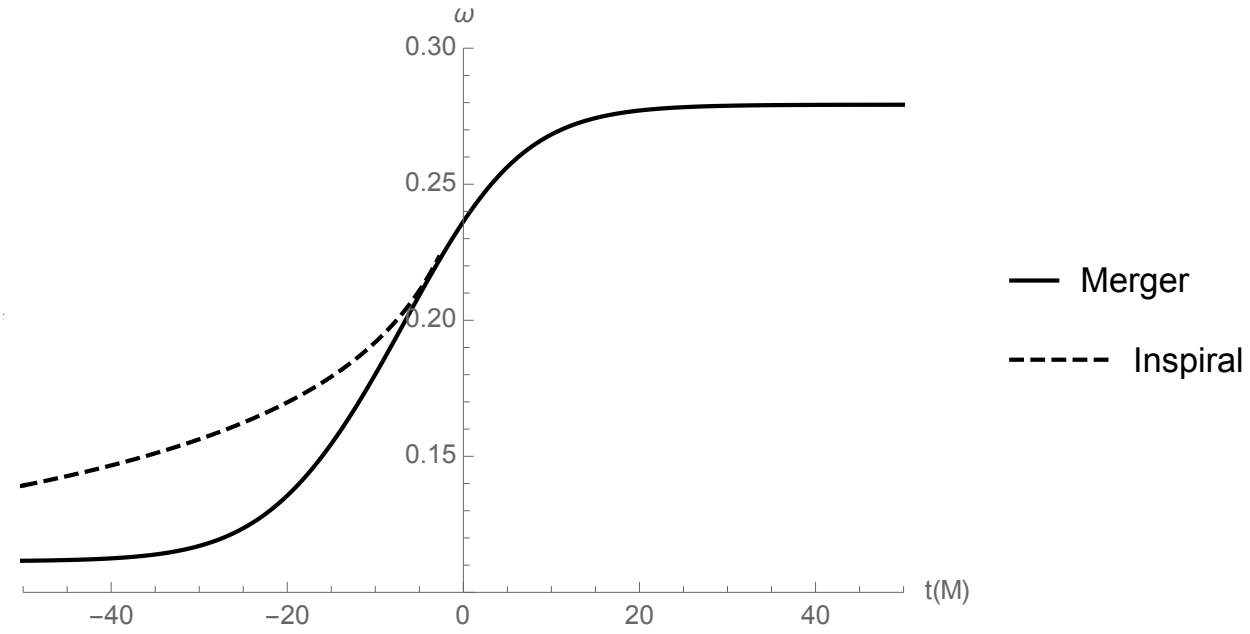

Figure 9: **Frequency Matching**.
The time evolution of the frequency, ω, for the end of our PN inspiral model and beginning of the BOB merger model. The inspiral frequency is time shifted backwards to find an overlap with the merger.

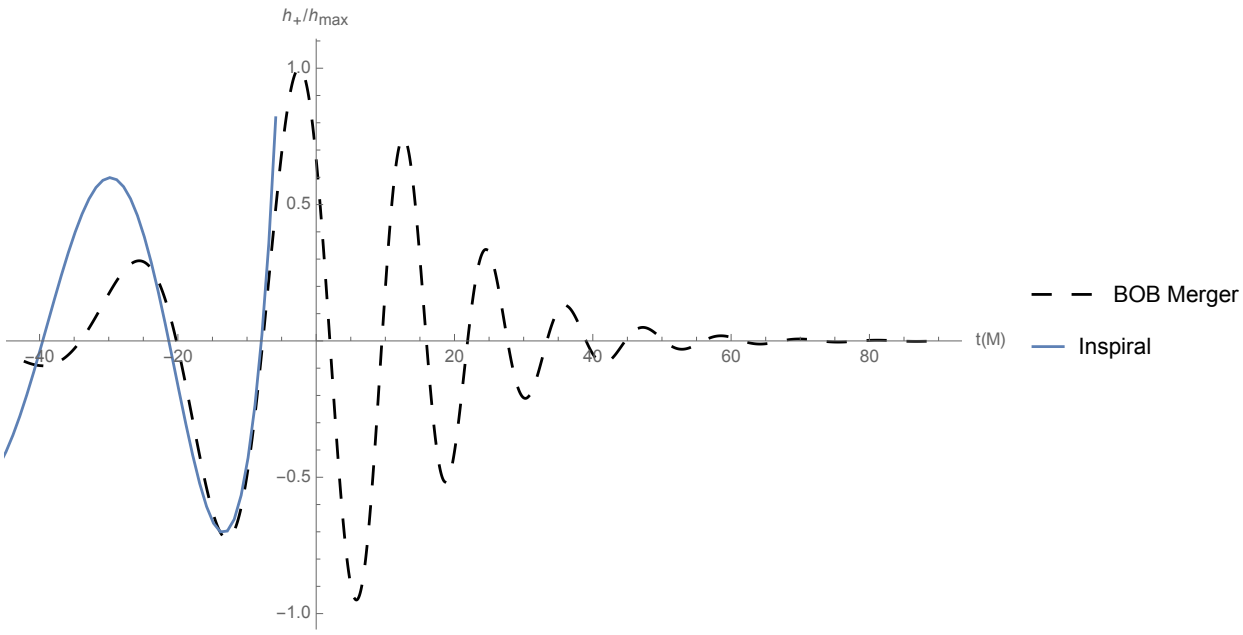

Figure 10: **Complete Waveform**.
The matching of the PN formulation for the strain of the inspiral phase with the BOB merger waveform model to create a complete strain waveform.

4.2 Merger Model Comparisons

We now want to compare the results of the BOB strain with those of the gIRS formulation that we coded in our previous work [7]. The gIRS model is formulated by tuning adjustable parameters and using fitting functions directly obtained by comparison with numerical relativity results. These models are formulated using units of time in solar masses. The results are obtained for a nearly equal mass case where the parameters are chosen from a numerical relativity simulation. Information on the parameters and the strain data for this simulation is taken from the SXS data bank that is easily accessible online. The SXS data will allow us to test our goal, which is to produce analytic results that are comparable to the widely accepted numerical relativity simulations. The initial masses for the specific SXS simulation that we chose for comparison are $m1 = 0.5000000618087954$ and $m2 = 0.4999999756534059$ in order to create a normalized total mass. The final spin (which appears in both gIRS and BOB formulation) is

$s_{fin} = 0.880726115$, and the final mass of the remnant black hole as a fraction of the total mass of the binary is $M_{fin} = 0.918682416261$. For consistency with the BOB formulation, we use equations (3.22) and (3.23) for the quality factor and the quasi-normal mode frequency in our gIRS calculations. Our comparison of the two merger models is shown in Figure 11. The merger models agree with each other throughout the merger and ringdown phases. Slight disagreement can be seen a few cycles before the peak, but this part of the merger model ends up being replaced by late inspiral modeling when creating a complete IMR waveform.

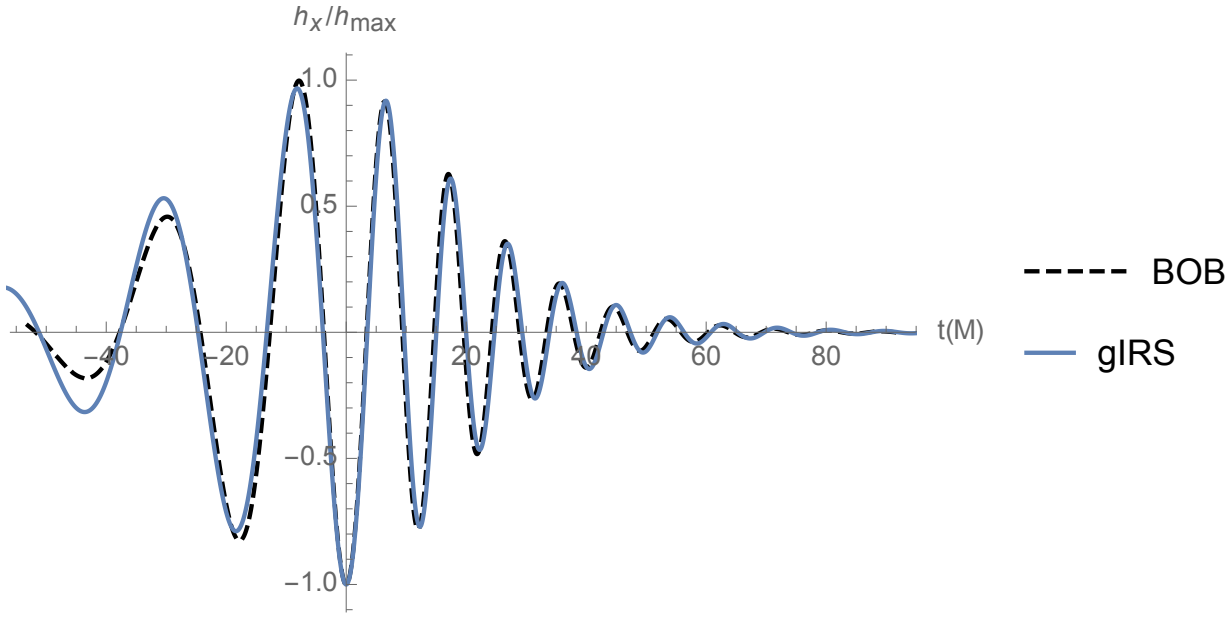

Figure 11: **BOB vs. gIRS Merger Strain**.
Comparison of the imaginary strain waveforms for the BOB and gIRS formulation for the nearly equal mass case. The peaks of the strains are normalized and both models are shifted to peak a time zero.

Since we know the models produce similar results, we can now see how the BOB model compares with the SXS data. This data is already expressed with time in units of solar masses, but the strain data is not normalized, and it does not peak at time zero. After shifting the SXS time data and normalizing the strain data, we are ready to compare our analytic results with the reliable and accepted numerical relativity data. This

comparison is shown in Figure 12.

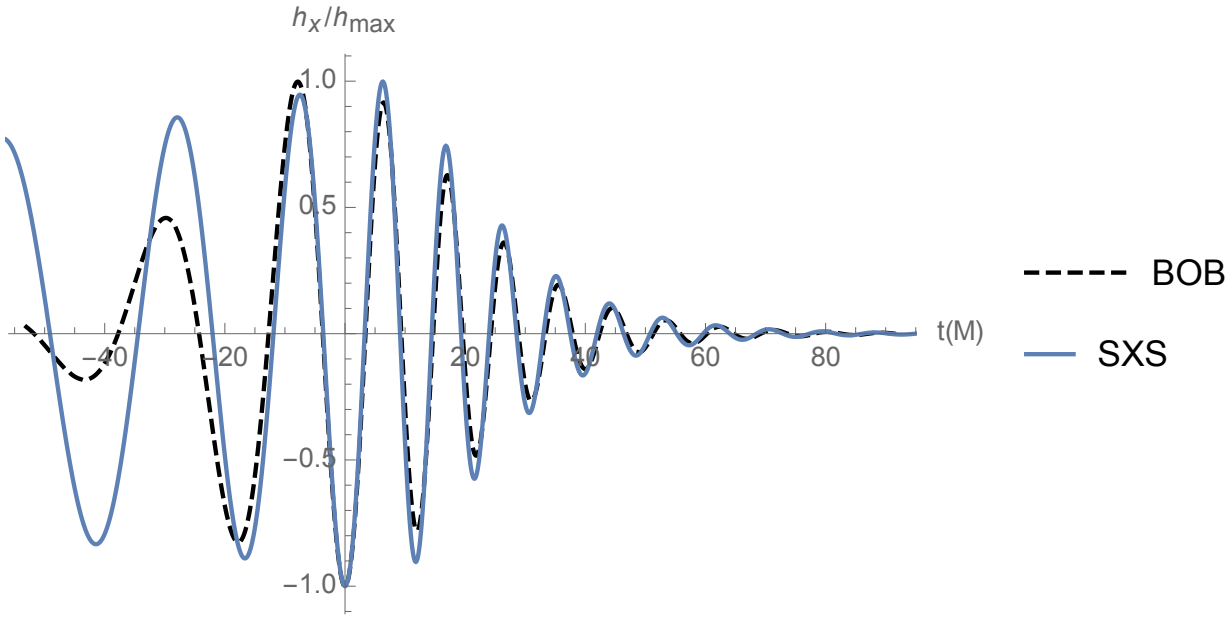

Figure 12: **BOB vs. SXS Merger Strain**.
Comparison of the imaginary strain waveform for the BOB formulation and the time shifted SXS imaginary strain data.

CHAPTER 5

CONCLUSIONS

Numerical relativity is the most reliable way to model the complex evolution of black hole binaries, but it has a major downfall. Simulating this problem is extremely computationally expensive and requires super computers, even for just one set of initial parameters. We need reliable simulations for a wide variety of parameters so that when a gravitational wave is detected, the detection can be compared with the available data to determine valuable information about the source of the signal. This issue has led to the development of analytic gravitational wave models for the inspiral and merger phases of the binaries' evolution. Since the merger phase is highly non-linear, a single model cannot describe both phases of the evolution, and separate models must be stitched together to produce a complete waveform. In this paper, we have successfully formulated a complete analytic waveform which gives results that match with numerical relativity simulations and is simple enough to evaluate on personal computers.

All BBH detections that have been confirmed up until now have only caught the end of the inspiral when the source has already circularized. However, with the improvements to the detectors discussed in the introduction, it is highly likely that LIGO and its partners will begin receiving detections early enough in the inspiral to see the eccentric behavior of the binary appear in the strain as extra harmonics. The expectation of eccentric detections was the purpose of developing an inspiral model that can describe moderately eccentric binaries. It was important to add the highest order PN corrections that are available because it allowed for us to push our inspiral models to a point where it circularizes enough to be matched with analytic merger models. Eccentricity calculations are computationally expensive so methods to speed up the time of evaluation were developed without any loss of accuracy. An example of one of these methods was the

polynomial interpolation that we used to express the eccentric anomaly. We tested the zero eccentricity limit of our eccentric model by comparing our results with the LOSC data for the first gravitational wave detection and found that our inspiral model is accurate.

The BOB model that we reproduced to describe the merger was developed based on the physical description of the problem and independent of the numerical relativity results (unlike the gIRS formulation). We discovered that both models produced nearly the same results. The gIRS formulation produced more cycles before the peak, but this data is not reliable, and we use the inspiral model to replace these cycles. More importantly, we found that these results agree with the numerical relativity SXS data when inputting the same initial parameters. The agreement of our analytic merger model with numerical relativity data is critical because the merger is much more difficult to model, but it is also where the most information about the source can be extracted. The ability to model the merger phase accurately while maintaining computational efficiency is one of the most exciting results of our work.

We have produced a completely analytic gravitational waveform that gives results that agree with both numerical relativity and actual gravitational wave detections. Analytic models such as these could replace the need for super computers to produce numerical relativity databanks, and instead, results for an even larger range of parameters could be produced using the more computationally efficient analytic models. As our ground-based detectors continue to improve, we expect to see a larger number of detections with a wider range of parameters. Although at the time no detections have been published for O3 (since they wait until after the entire observation run is complete before publication), promising candidates have been detected around one or two times a week on average. The rate of detections is a much higher frequency than previous observation runs and emphasizes the importance of having readily available databanks!

The current observation run will end in April 2020 and if any eccentric binaries are confirmed, the inspiral model could be compared with the published data that will follow.

Since the matching is done manually, it would be beneficial to develop a method of matching that is done automatically without altering the script when the code is evaluated.

REFERENCES

[1] K. G. Arun, Luc Blanchet, Bala R. Iyer, and Siddhartha Sinha, *Third post-newtonian angular momentum flux and the secular evolution of orbital elements for inspiralling compact binaries in quasi-elliptical orbits*, Physical Review D **80** (2009), no. 12.

[2] John G. Baker, William D. Boggs, Joan Centrella, Bernard J. Kelly, Sean T. McWilliams, and James R. van Meter, *Mergers of nonspinning black-hole binaries: Gravitational radiation characteristics*, Physical Review D **78** (2008), no. 4.

[3] Emanuele Berti, Vitor Cardoso, and Clifford M. Will, *Gravitational-wave spectroscopy of massive black holes with the space interferometer LISA*, Physical Review D **73** (2006), no. 6.

[4] Yannick Boetzel, Abhimanyu Susobhanan, Achamveedu Gopakumar, Antoine Klein, and Philippe Jetzer, *Solving post-newtonian accurate kepler equation*, Physical Review D **96** (2017), no. 4.

[5] Michael Boyle, Daniel Hemberger, Dante A B Iozzo, Geoffrey Lovelace, Serguei Ossokine, Harald P Pfeiffer, Mark A Scheel, Leo C Stein, Charles J Woodford, Aaron B Zimmerman, Nousha Afshari, Kevin Barkett, Jonathan Blackman, Katerina Chatziioannou, Tony Chu, Nicholas Demos, Nils Deppe, Scott E Field, Nils L Fischer, Evan Foley, Heather Fong, Alyssa Garcia, Matthew Giesler, Francois Hebert, Ian Hinder, Reza Katebi, Haroon Khan, Lawrence E Kidder, Prayush Kumar, Kevin Kuper, Halston Lim, Maria Okounkova, Teresita Ramirez, Samuel Rodriguez, Hannes R Rüter, Patricia Schmidt, Bela Szilagyi, Saul A Teukolsky, Vijay Varma, and Marissa Walker, *The SXS collaboration catalog of binary black hole simulations*, Classical and Quantum Gravity **36** (2019), no. 19, 195006.

[6] Alessandra Buonanno and Thibault Damour, *Transition from inspiral to plunge in binary black hole coalescences*, Physical Review D **62** (2000), no. 6.

[7] Dillon Buskirk and Maria C Babiuc Hamilton, *A complete analytic gravitational wave model for undergraduates*, European Journal of Physics **40** (2019), no. 2, 025603.

[8] Marco Celoria, Roberto Oliveri, Alberto Sesana, and Michela Mapelli, *Lecture notes on black hole binary astrophysics*, 2018.

[9] Peter Colwell, *Bessel functions and kepler's equation*, The American Mathematical Monthly **99** (1992), no. 1, 45–48.

[10] Ian Hinder, Frank Herrmann, Pablo Laguna, and Deirdre Shoemaker, *Comparisons of eccentric binary black hole simulations with post-newtonian models*, Physical Review D **82** (2010), no. 2.

[11] E. A. Huerta, Prayush Kumar, Bhanu Agarwal, Daniel George, Hsi-Yu Schive, Harald P. Pfeiffer, Roland Haas, Wei Ren, Tony Chu, Michael Boyle, Daniel A. Hemberger, Lawrence E. Kidder, Mark A. Scheel, and Bela Szilagyi, *Complete waveform model for compact binaries on eccentric orbits*, Physical Review D **95** (2017), no. 2.

[12] Nicholas Loutrel, Samuel Liebersbach, Nicolás Yunes, and Neil Cornish, *The eccentric behavior of inspiralling compact binaries*, Classical and Quantum Gravity **36** (2018), no. 2, 025004.

[13] Sean T. McWilliams, *Analytical black-hole binary merger waveforms*, Physical Review Letters **122** (2019), no. 19.

[14] David L. Meier, *Black hole astrophysics*, Springer Berlin Heidelberg, 2012.

APPENDIX A

APPROVAL LETTER

MARSHALL UNIVERSITY
www.marshall.edu

Office of Research Integrity

November 5, 2019

Dillon Buskirk
1314 39th Street
Parkersburg, WV 26104

Dear Mr. Buskirk:

This letter is in response to the submitted thesis abstract entitled *"Analytically Modeling Eccentric Binary Black Holes: From Inspiral to Merger."* After assessing the abstract, it has been deemed not to be human subject research and therefore exempt from oversight of the Marshall University Institutional Review Board (IRB). The Code of Federal Regulations (45CFR46) has set forth the criteria utilized in making this determination. Since the information in this study does not involve human subjects as defined in the above referenced instruction, it is not considered human subject research. If there are any changes to the abstract you provided then you would need to resubmit that information to the Office of Research Integrity for review and a determination.

I appreciate your willingness to submit the abstract for determination. Please feel free to contact the Office of Research Integrity if you have any questions regarding future protocols that may require IRB review.

Sincerely,

Bruce F. Day

Bruce F. Day, ThD, CIP
Director

WE ARE...MARSHALL.
One John Marshall Drive • Huntington, West Virginia 25755 • Tel 304/696-4303
A State University of West Virginia • An Affirmative Action/Equal Opportunity Employer

APPENDIX B

Interpolation Code

```
u3PNADMtable = Table[u3PNADM[t], {t, 0, Tfin, dt}];

u3PNADMvstime = Partition[Riffle[tArray, u3PNADMtable], 2];

u3PNADMvstime1 = MapAt[Delete[#, 0] &, u3PNADMvstime, {All, 2}];

u3PNADMinterp = Interpolation[u3PNADMvstime1,
  InterpolationOrder → 4]
```

Figure 13: **Mathematica Interpolation**.
The first line tabulates the values for u. The second creates the table (t, u). The third removes an extra pair of brackets around u values so that the table is in a form that can be used by the interpolation command in the fourth line.